The Spatiotemporal Variations of Total Column Ozone Concentration over Ethiopia

Abebaw Bizuneh Alemu (abebaw08@gmail.com)
Bahir Dar University https://orcid.org/0000-0002-0719-6136
Abdu Mohammed Seid
Bahir Dar University
Baylie Damtie Yeshita
Kepler College
U. Jaya Prakash Raju
Bahir Dar University

Research Article

Keywords: Total Column Ozone , Dobson Unit, Ozone Concentration, OMPS Satellite, Timeseries, Ethiopia

Posted Date: July 5th, 2022

DOI: https://doi.org/10.21203/rs.3.rs-1754598/v1

RESEARCH

The Spatiotemporal Variations of Total Column Ozone Concentration over Ethiopia

Abebaw Bizuneh Alemu[1,3*], Abdu Mohammed Seid[2], Baylie Damtie Yeshita[1] and U. Jaya Prakash Raju[1]

Abstract

We have studied the spatiotemporal characteristics of ozone concentration over Ethiopia using Ozone Mapper and Profiling Suite (OMPS) Satellite measurements. Daily total column ozone measurements of 252 data points with spatial resolution $1^\circ \times 1^\circ$ for the study area and its surrounding during the period 2012 – 2020 have been analyzed. We investigated the spatial variation over the region from longitudinal and latitudinal bands separately by assessing existence of mean difference among different bands using multicomparison analysis of variance technique and determined the clusters in the region. For the temporal variability, we employed timeseries analysis and decomposed the ozone concentration series for each class into seasonal, trend and residual components. We have found that the total column ozone concentration has a maximum value of $301\mathrm{DU}$ during summer on August 18, 2013 and a minimum value of $216\mathrm{DU}$ during winter on January 03, 2013 over the study period. The 95% confidence level of the overall mean of total column ozone concentration during the study period was found to be $(261.28 \pm 4.2)\mathrm{DU}$. Our spatial data analysis revealed that the spatial distribution of ozone over Ethiopia can be classified into three major regions: Southern Cluster $(4.5^\circ N - 8.5^\circ N$ & $32.5^\circ E - 47.5^\circ E)$, North–Eastern Cluster $(9.5^\circ N$ to $14.5^\circ N$ & $41.5^\circ E - 47.5^\circ E)$ and North–Western Cluster $(9.5^\circ N - 14.5^\circ N$ & $32.5^\circ E - 40.5^\circ E$). We also checked the degree of determination among bands in same cluster to see if the concentration of ozone in one band can be explained by the concentration in a another band for each cluster and confirmed the reliability of the classification. From the timeseries analysis, we made an assessment of spectral periodogram for each cluster and obtained a single Fourier power peak with frequency of $f = 0.002768Hz$, which indicated that the ozone concentration has an annual cyclic behavior in the region. A truncated Fourier series fit is made to determine the annual seasonal component. The non-parametric Mann-Kendall's trend test with a 95% confidence level of significant indicated a decreasing linear trend with a depletion rate of 0.77 DU/yr, 0.73 DU/yr, and 0.43 DU/yr over North–Western, North–Eastern & Southern clusters respectively. The analysis of residuals result for each cluster indicated that the standardized residuals are normally distributed and white noises. Hence, the model considered is reliable.

Keywords

Total Column Ozone , Dobson Unit, Ozone Concentration, OMPS Satellite, Timeseries, Ethiopia

*Correspondence:
abebaw08@gmail.com
[1]Bahir Dar University, Collage of Science, Department of Physics, Ethiopia
Full list of author information is available at the end of the article

1 Introduction

Ozone is chemically very active colorless gas which reacts with a great many other substances. It plays a vital role in controlling the chemical composition and climate of the atmosphere (Kambezidis et al., 1998; Rafiq et al., 2017; Rex et al., 2004). These characteristics of ozone implies that ozone can be considered as harmful and good depending on its function. The function of ozone vary depending on its location in the atmosphere and its level of concentration. Ozone is found primarily in two regions of the atmosphere. About 10 % of atmospheric ozone is found in the troposphere, the region from the surface of the earth up to 10km altitude, while the remaining 90 % is found in the stratosphere, the region between the top of the troposphere till about 50 km altitude. Stratospheric ozone is useful in absorbing

the dangerous ultraviolet radiation from the sun and protects living things below it. Near the Earth's surface, the ozone's reactive nature can damage ecosystems when it is beyond the natural background level. For instance, in this region it can cause rubbers to crack, hurt plants and results in respiratory diseases in humans etc. These characteristics and associated functions of ozone in the atmosphere necessitates the need to investigate ozone concentration and its corresponding dynamics both locally and globally.

Total column ozone at any location is found by measuring all the ozone in the atmosphere directly above that location using ground-based stations and satellites. The total column ozone (TCO) is the total amount of atmospheric ozone up to the height of the stratopause and is measured as an integrated values of ozone over the column of unit cross-section. The TCO concentration amounting less than 220 DU are usually considered as an indicator of ozone hole formation (Berbert et al., 1977; Standard, 2019). The ozone hole has gained worldwide attention and this is due to its association with harmful effects of UV rays including cancer risks and effects on plants and animals. Over exposure to ultraviolet radiation from the sun is one of the major reasons for skin cancer (Anwar et al., 2016; LoConte et al., 2018; Sivasakthivel and Reddy, 2011). Thus, the assessment of the state of ozone concentration together with the study of its spatiotemporal dynamics from satellite data has become a major topic of research to monitor ozone and safeguard our environment (Aucamp et al., 2011; Chipperfield, 2003; Liu et al., 2010; Ogunniyi and Sivakumar, 2018).

Many studies have been done on the spatiotemporal dynamics of TCO both globally and locally. For example, (Rafiq et al., 2017; Staehelin et al., 2001) have shown a decreasing trends in TCO concentration in the middle and high latitudes of both hemispheres. (Berbert et al., 1977) also have shown that the levels of ozone near the equatorial regions is lower than the global average value of $\approx$ 300 DU. This might be associated with the position of the sun over the tropics as the sun is assumed to be the dominant source of variation of TCO and the dynamics of tropical atmosphere (Madhu et al., 2016). Studying the variations of ozone concentration over a specific region plays an important role in understanding the environmental conditions including estimating the level of exposure to ultraviolet radiation.

(Rafiq et al., 2017) analysed the seasonal and inter-annual variations of TCO over Pakistan region from AQUA-AIRS Level-3 Daily Global satellite data during 2003–2011. They used simple averages to determine the monthly, inter-annual and annual TCO variations. Their study indicated that in Northern Pakistan region, $30^{\circ}N - 37^{\circ}N$, the maximum ozone concentration occurs in winter (DJF) season and the minimum in summer (JJA). Whereas, in southern part of Pakistan, $(23^{\circ}N - 29^{\circ}N)$, they have shown that the highest ozone level was recorded in the summer while the lowest record was in the winter season. (Chen et al., 2014) also investigated the spatiotemporal variability of TCO over the Yangtze River Delta, the most populated region in China, using TCO data from the Total Ozone Mapping Spectrometer (TOMS) for the period 1978–2005 and from Ozone Monitoring Instrument (OMI) for the period 2004–2013. They computed coefficient of relative variation for each latitudinal and longitudinal band to quantify the spatial variability and modelled the seasonality as an annual cycle with a sinusoidal function.

Their study didn't explain why the authors consider annual cycle in the seasonality, instead they simply fit the data with an annual periodic sinusoidal function. In such a study, determining a correct seasonal behaviour is crucial as the seasonality might also affect the trend analysis result. This is so, as trend analysis is mostly done on the deseasonalized data. In this regard, we are interested to assess spectral periodogram of TCO timeseries to determine the Fourier power peak and corresponding frequencies to alleviate such problems as this could determine seasonalities from timeseries data correctly. In the current study, we aim to investigate the spatiotemporal dynamics of TCO over Ethiopia from daily TCO satellite measurements obtained from OMPS during the period 2012–2020. Thus, the aim of the current study is twofold generally. The first objective is to determine if the region can be classified into subregions based on the overall TCO mean along latitude and longitude through mean difference tests and multiple group comparison tests. The second objective is to make timeseries analysis of TCO for each cluster. Here, we intend to decompose the TCO series into seasonal, trend and residual components. Such local studies on spatiotemporal variation of TCO are crucial to monitor TCO concentration associated impacts locally and for many environmental and health related policy discussions locally. Since Ethiopia lies within the tropical latitudes, where there is more ultraviolet radiation over the equator compared to high latitudes (Bais et al., 2006), continuous monitoring of TCO concentration is fundamental. Moreover, ozone concentrations over the tropics is highly linked with the dynamical process of the tropical atmosphere which necessitates the need to characterize TCO distribution over different regions of Ethiopia.

The rest of this paper is organized as follows: In Section 2, we start by presenting data sources and the study area followed by discussions of the method used for the spatial clustering and timeseries analysis of the TCO. In section 3, we have given a detailed discussion of the results obtained in the study. Finally, in Section 4, we conclude the study.

2 The Study Area and Data Analysis

Study Area

Ethiopia is located in the North-Eastern part of Africa, which lies approximately between $3^{\circ}N$ & $15^{\circ}N$ latitude and $33^{\circ}E$ & $48^{\circ}E$ longitude. There are four seasons in Ethiopia including winter (DJF), spring (MAM), summer (JJA) and autumn (SON). The topography of Ethiopia is highly diverse, with an elevation ranging from 125 m below sea level in the Danakil depression to 4620 m above sea level in Ras Dashen mountain range. The climate varies with altitude, from the arid to cool climate of the plateau. It is useful to study the characteristics of ozone concentration over this region with such a diverse topography and climate to see its variation accordingly.

In this study, we have considered 108 data points of OMPS satellite measurements in the study area as indicated in Fig. 1 and 144 data points from the neighbourhood of Ethiopia. The OMPS satellite was built by Ball Aerospace & Technologies Corporation for measuring the concentration of ozone in the Earth's atmosphere (Dittman et al., 2002; Veefkind et al., 2006). The data were obtained from NASA Goddard Space Flight Center Website for a period ranging 2012 - 2019 with $1^{\circ} \times 1^{\circ}$

resolution and which have been already validated for the study area by (Takele Kenea et al., 2013). We used a bi-linear interpolation in order to obtain estimates for few missing data points as suggested by (Berbert et al., 1977).

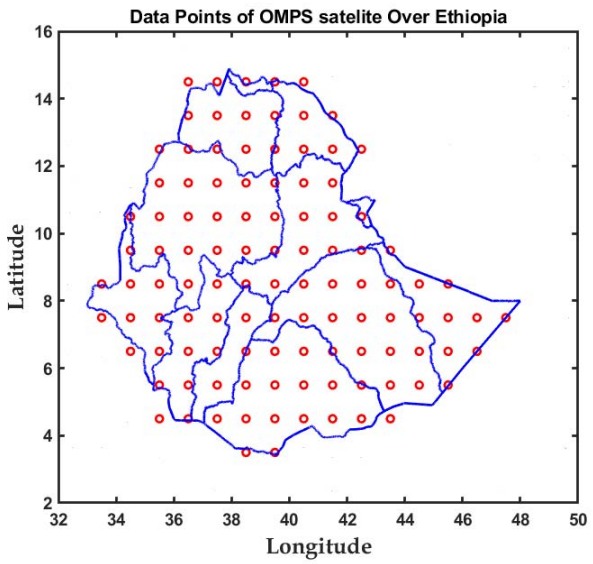

Figure 1 Data points of OMPS satellite over Ethiopia, it has 15 columns and 12 rows as longitudinal and latitudinal bands respectively.

Data Analysis Method

The characteristics of TCO distribution over Ethiopia is presented by classifying the region into sub-regions or clusters based on the levels of TCO concentration and by carrying out timeseries analysis of TCO for cluster. We have classified the entire area into some representative sub-regions using spatial data clustering technique. Particularly, we employed mean difference tests of analysis of variance followed by multiple group comparison tests for the spatial clustering. This is possible by using fifteen longitudinal and twelve latitudinal bands data over the region by considering measurement values along same longitude as a longitudinal band and data values along same latitude as a latitudinal band, respectively. In order to study the longitudinal integrated temporal variations of ozone as a function of a latitude band, we denote the ozone measurements for the i^{th} latitudinal band at time t by $C_{t,i}$. We can then express the latitudinal and temporal varying measurement matrix $\mathbf{C}_{\text{lat}}$ by

$$\mathbf{C}_{\text{lat}} = \left(C_{t,i}\right)_{2890\times 12} = \begin{pmatrix} C_{1,1} & C_{1,2} & \dots & C_{1,12} \\ C_{2,1} & C_{2,2} & \dots & C_{2,12} \\ \vdots & \vdots & \dots & \vdots \\ C_{2890,1} & C_{2890,2} & \dots & C_{2890,12} \end{pmatrix} \tag{1}$$

where $C_{t,i}$ is the longitudinal integrated TCO measurement over the i^{th} latitudinal band at time t, and $i = 1, 2, \dots, 12$ denotes the latitudinal bands that corresponds

with $3.5°, 4.5°, \ldots, 14.5°$ North and $t = 1, 2, \ldots, 2890$ represents time, which is the days of the year in the study period from February 2012 to December 2019.

Similarly, to study longitudinal variations of ozone, we use the longitudinal and temporal varying measurement matrix, denoted as $\mathbf{C}_{\text{lon}}$, and it is given by

$$\mathbf{C}_{\text{lon}} = \left(C_{t,j}\right)_{2890\times 15} = \begin{pmatrix} C_{1,1} & C_{1,2} & \ldots & C_{1,15} \\ C_{2,1} & C_{2,2} & \ldots & C_{2,15} \\ \vdots & \vdots & \ldots & \vdots \\ C_{2890,1} & C_{2890,2} & \ldots & C_{2890,15} \end{pmatrix} \tag{2}$$

where $C_{t,j}$ is the latitudinal integrated TCO measurement over the j^{th} longitudinal band at time t, and $i = 1, 2, \ldots, 15$ denotes the longitudinal bands that corresponds with $33.5°, 34.5°, \ldots, 47.5°$ East and $t = 1, 2, \ldots, 2890$ represents time, which is the days of the year in the study period from February 2012 to December 2019.

We can now classify the TCO distribution over Ethiopia into sub-regions by assessing the existence of mean difference between the measurement values. This is carried out by using the analysis variance technique (Hamada and Wu, 2000; Kutner et al., 2005), which can be described by

$$F = \left(\frac{\sum_j n_j(\bar{C}_j - \bar{C})^2}{\sum_j \sum_t (C_{t,j} - \bar{C}_j)^2}\right)\left(\frac{N-k}{k-1}\right), \tag{3}$$

where n_j, $C_{t,j}$, N, $\bar{C}$, $\bar{C}_j$, k, and F refers the number of observations on j^{th} band, values of integrated TCO value for j^{th} band at time t, total number of observations over all bands, overall mean of TCO, mean of TCO for j^{th} band, total number of bands and variation between sample means respectively. By comparing F values with the critical value of F at 95% confidence level, we can classify the observation points based on the result of analysis of variance into a particular cluster. The analysis of variance method tells us whether there is a mean difference or not between the clusters. However, it doesn't tell us whether the concentration of total column ozone in one cluster can be explained by the concentration in a another cluster. For the degree of determination of ozone concentration among clusters, we use the degree of determination directly, which can be expressed by

$$R^2_{j,k} = \frac{\left(\sum_i C_j C_k - N\bar{C}_j\bar{C}_k\right)^2}{\left(\sum_i C_j^2 - N\bar{C}_j^2\right)\left(\sum_i C_k^2 - N\bar{C}_k^2\right)}, \tag{4}$$

where N, C_j, C_k, $\bar{C}_j, \bar{C}_k$, and $R^2_{j,k}$ refers the number of data pairs, values of integrated TCO value for j^{th} band, values of integrated TCO value for k^{th} band, mean of TCO for j^{th} band, mean of TCO for k^{th} band and the coefficent of determination between j^{th} and k^{th} bands respectively.

Timeseries analysis for all the clusters was carried out independently from the mean values of all the observations in that particular cluster for each day of the year. Here, we decomposed the daily timeseries data from each cluster into seasonal, trend and residual components. We didn't consider other cyclic component in our

definition as we are working with a short period of data (only eight years data). Hence, we defined the timeseries with additive components as:

$$Y_t = S_t + T_t + \varepsilon_t, \tag{5}$$

where T_t, S_t and ε_t are the trend, Seasonal or Cyclic variation and residual components, respectively of the mean value data Y_t corresponding to each cluster.

Before defining the trend, we would like to check its existence and behavior through non-parametric Mann Kendall test. The Mann-Kendall test can capture a highly significant trend (Libiseller et al., 2005). The main advantage of this method is that it is not sensitive to outliers and the data do not need to conform to any particular distribution. The Mann-Kendall test is described mathematically as

$$S = \sum_{i=1}^{n-1} \sum_{j=i+1}^{n} sgn(X_j - X_i), \tag{6}$$

for

$$sgn(X_j - X_i) = \begin{cases} 1 & \text{if } X_j - X_i > 0, \\ 0 & \text{if } X_j - X_i = 0, 1 \leq i < j \leq n, \\ -1 & \text{if } X_j - X_i < 0 \end{cases} \tag{7}$$

where X_j and X_i refer to TCO concentration at the j^{th} and i^{th} time respectively. The corresponding variance is

$$\sigma^2 = \frac{1}{18}(n(n-1)(2n+5) - \sum_{j=1}^{p} t_j(t_j-1)(2t_j+5)), \tag{8}$$

where p refers the number of the tied groups and t_j is the number of data points in the j^{th} tied group. Then, the standardized test statistic Z is computed by

$$Z = \begin{cases} \frac{S-1}{\sigma} & \text{if } S > 0, \\ 0 & \text{if } S = 0, . \\ \frac{S+1}{\sigma} & \text{if } S < 0 \end{cases} \tag{9}$$

The presence of a statistically significant trend is evaluated from the Z value and the null hypothesis is rejected if the absolute value of Z is larger than the theoretical value $Z_{1-\alpha}$, where $\alpha = 0.05$ is considered as the statistical significance level. The long term increasing or decreasing pattern of TCO timeseries have been modeled using linear trend in Africa (Oluleye and Okogbue, 2013). In this study, we also considered a linear trend for the eight years data, defined it as

$$T_t = \gamma t + \alpha_0, \tag{10}$$

where γ and α_0 are the slope and intercept of the trend line to be determined from the data respectively.

The cyclic fluctuation of the timeseries is the best fit of the daily de-trended TCO timeseries data (Antón et al., 2011; Fioletov et al., 2008). The seasonality or cyclic fluctuation component of TCO timeseries is usually modeled with a one term Fourier series model (Chen et al., 2014; Schmalwieser et al., 2003). The main challenge here is on determining the period of the cycle. We used power spectrum Fast Fourier transform (FFT) on the de-trended data to identify the dominant frequency. In our case, we get only one dominant frequency which accounts with the annual periodicity of the seasonality in the TCO series. We defined the cyclic component of the TCO as

$$S_t = \alpha_0 + \sum_{i=1}^{n} \alpha_i.sin(i.\omega t) + \sum_{i=1}^{n} \beta_i.cos(i.\omega t), \tag{11}$$

where t refers the time in days of year, α_i,and β_i are free parameters to be determined from the data and $\omega = 2\pi f$, where f is the dominant frequency from FFT.

We defined the residual component by de-trending and de-seasonalizing the data as

$$\epsilon_t = Y_t - S_t - T_t. \tag{12}$$

Even though it is unlikely to observe other cyclic components of TCO timeseries in such a short period of time, one could check the existence of the other cyclic fluctuations part in the residual component after the trend and seasonal components are removed. We discussed the results obtained when we implement the methods discussed on the daily TCO data from 2012-2020 in the subsequent sections.

3 Results and Discussions

3.1 Spatial Variations of TCO

3.1.1 Latitudinal TCO Variations

We have studied the latitudinal variations of TCO by calculating the daily difference of TCO value between the northern most region of Ethiopia with TCO data ($14.5^{\circ}N$) and the values at other eleven latitudinal bands sequentially. We used the degree of determination parameter (R^2) using Equation (4). These yield the standard deviations and the degree of determination parameter values for latitudinal band differences as in Table 1.

The tabular values indicate that the statistical differences between the value of TCO at the northernmost latitude of Ethiopia and its value at other lower latitude bands increases as the distance of separation increases. The degree of determination parameter (R^2) between TCO value at the northernmost latitude and other bands demonstrates similar results. We can see that the values of the coefficient of determination measures the strength of the relationship between TCO characteristics at the northern most latitude region and other latitudinal bands.

According to (Akoglu, 2018), a value of $R^2 > 0.8$ indicates a strong relationship between the two observation points. Table 1 shows that the values of R^2 vary

Table 1 Statistical parameters that depict the difference between the mean daily TCO value at northern most latitude $(14.5°N)$ and other latitudinal bands over Ethiopia

Latitude	Std	$\mu_1 - \mu_2$	R^2
$14.5° - 13.5°$	1.6	0.5	0.989
$14.5° - 12.5°$	2.7	1.57	0.969
$14.5° - 11.5°$	3.74	3.29	0.942
$14.5° - 10.5°$	4.75	3.56	0.907
$14.5° - 9.5°$	5.75	3.71	0.864
$14.5° - 8.5°$	6.77	3.5	0.809
$14.5° - 7.5°$	7.78	3.0	0.742
$14.5° - 6.5°$	8.74	2.73	0.668
$14.5° - 5.5°$	9.58	1.86	0.596
$14.5° - 4.5°$	10.39	1.8	0.526
$14.5° - 3.5°$	11.14	0.86	0.461

from 0.99 to 0.47. This means that the observation at $(14.5°N)$ can be taken as a statistical representations of TCO values up to 7.5° indicating similarities in TCO values over 7° latitude coverage.

3.1.2 Longitudinal TCO Variation

Similarly the longitudinal variations of TCO have been investigated by evaluating the statistical difference between the mean daily value of TCO observed over the most Eastern tip of Ethiopia with TCO data (47.5^oE) and TCO values over other lower longitudinal regions. Table 2 shows the standard deviations, mean and the degree of determination (R^2) for the respective bands.

Table 2 Statistical parameters that depict the difference between TCO daily mean value at 47.5^o and its value at other lower longitudinal bands.

Longitude	Std	$\lvert\mu_1 - \mu_2\rvert$	R^2
$47.5^o - 46.5^o$	2.91	1.01	0.946
$47.5^o - 45.5^o$	2.21	0.45	0.969
$47.5^o - 44.5^o$	3.47	1.80	0.924
$47.5^o - 43.5^o$	3.11	1.49	0.939
$47.5^o - 42.5^o$	4.09	1.85	0.895
$47.5^o - 41.5^o$	4.2	0.54	0.893
$47.5^o - 40.5^o$	4.73	5.48	0.863
$47.5^o - 39.5^o$	4.59	1.98	0.871
$47.5^o - 38.5^o$	4.83	5.2	0.854
$47.5^o - 37.5^o$	4.88	6.26	0.855
$47.5^o - 36.5^o$	5.27	2.83	0.825
$47.5^o - 35.5^o$	5.1	5.18	0.836
$47.5^o - 34.5^o$	5.95	1.08	0.777
$47.5^o - 33.5^o$	5.87	2.67	0.783

Table 2 shows that all values of R^2 is greater than 0.8. This means that the observation at 47.5^o can well represent TCO observations up to 33.5^o. In order to map out regions with similar TCO values in more details, we have used spatial clustering technique.

3.2 Clustering TCO measurements over Ethiopia

It is practical to classify the entire data points into representative sub-regions and investigate the distribution of TCO measurements at different topographical and climate zones of Ethiopia. We carried out the clustering of TCO values for the study area using Equation (3). We give the discussion for the longitudinal and latitudinal clusters in the subsequent subsections.

3.2.1 Longitudinal Clustering

We used the null hypothesis to classify the TCO corresponding to specific longitudinal band in time. We defined the null hypothesis here as follows.

- H_0: There is no mean difference between any two longitudinal bands,
- H_1: There is mean difference at least between two of the longitudinal bands.

We demonstrate the mean difference among longitudinal bands in Table (3) below.

Table 3 A table demonstrating mean difference among longitudinal bands

Source	SS	df	MS	F	P
Groups	13867	14	990.3	67.06	< 0.001
Error	599662	40600	14.77		
Total	613529	40614			

The value $p < 0.05$ in Table (3) indicates that the mean TCO distributions over different longitudinal bands have a significant difference. This means that we obtained enough evidence to reject the null hypothesis. We have carried out a multiple comparison technique to investigate the difference among TCO measurements at different longitude bands as shown in Table (4).

Table 4 Longitudinal statistical variations of TCO measurements

Lon(^{o})	Lon(^{o})	Lower Limits	$\lvert\mu_1 - \mu_2\rvert$	Upper Limits	p-value
42.5	47.5	1.733	1.85	1.967	0.150
42.5	46.5	-0.901	0.218	1.338	1.000
42.5	45.5	-0.554	0.567	1.687	0.930
42.5	44.5	-1.219	-0.099	1.020	1.000
42.5	43.5	-1.35	-0.23	0.890	1.000
42.5	41.5	-1.537	-0.417	0.703	0.996
42.5	40.5	-0.356	0.358	1.073	0.895
39.5	38.5	-0.782	0.338	1.458	0.990
39.5	37.5	-0.200	0.92	2.04	0.255
39.5	35.5	-2.021	-0.901	0.219	0.287
39.5	36.5	-0.510	0.61	1.73	0.880
39.5	34.5	-1.744	-0.624	0.496	0.859
39.5	33.5	-1.159	-0.039	1.081	1.000

We can see from Table (4) that the study area can be divided into two sub-regions based on the characteristics of TCO measurements as Western cluster covering the regions from $33.5^\circ E$ to $39.5^\circ E$ and Eastern cluster covering the region $40.5^\circ E$ to $47.5^\circ E$. A similar procedure follows for the latitudinal clustering as discussed below.

3.2.2 Latitudinal Clustering

Following the null hypothesis defined in the previous subsection but for latitudinal bands, we have carried out a similar investigation in order to cluster TCO measurements at different latitude bands.

Table 5 A table for testing mean difference along latitudinal bands

Source	SS	df	MS	F	P
Groups	5886.1	11	535.1	33.26	0.00001
Error	523670	32546	16.09		
Total	529556	32557			

The value $p \leq 0.01$ in Table (5) shows that the average TCO measurements along different latitudinal bands differ significantly and this means that our null

hypothesis is rejected. We have carried out multiple comparison technique to study the level of statistical difference among TCO measurements over different latitudinal bands as shown in Table (6).

Table 6 A table for testing mean difference along latitudinal variation

Lat(^{o})	Lat(^{o})	Lower Limits	$\lvert\mu_1 - \mu_2\rvert$	Upper Limits	p-value
13.5	14.5	0.4394	0.4960	0.5526	0.9606
13.5	12.5	-0.0831	1.0613	2.2057	0.0997
13.5	11.5	-1.7109	-0.5669	0.5772	0.9025
13.5	10.5	-1.9826	-0.8386	0.3055	0.4090
13.5	9.5	-2.1184	-0.9747	0.1690	0.1862
13.5	3.5	-0.8203	0.3242	1.4686	0.9989
6.5	8.5	-1.9065	-0.7627	0.3810	0.5647
6.5	7.5	-1.4069	-0.2632	0.8805	0.9998
6.5	5.5	-2.0219	-0.8780	0.2658	0.3342
6.5	4.5	-2.0874	-0.9434	0.2007	0.2286

Table (6) depicts results of the multiple comparisons analysis. The comparisons clearly show that the study area can be divided into two sub-regions based on the statistical difference of the TCO measurements over different latitude as Southern region covering $4.5°$ to $8.5°N$ and Northern region that covers $9.5°$ to $14.5°N$.

3.2.3 Multiple Clustering

The discussions in the previous subsections on latitudinal and longitudinal clusters reveals the existence of two clusters for each latitudinal and longitudinal bands as Northern and Southern clusters for latitudinal bands, and Eastern and western clusters for longitudinal bands. It is useful to study if a given cluster itself can be represented by another cluster as the classifications above have been done by considering one dimension and that is through the latitudinal or longitudinal bands at a time. Classification through two dimensional space allows proper mapping of TCO for practical implication. We consider NW, NE, SW, SE regions for multiple clustering. Classification of clusters can be studied by means of multiple clustering method following the approach by (Boulis and Ostendorf, 2004). The statistical parameters obtained by multiple clustering analysis of the clusters are presented in Table (7).

Table 7 Statistical parameters obtained by multiple clustering.

Groups	Groups	Lower Limits	$\mu_1 - \mu_2$	Upper Limits	p-value
NW	NE	2.3599	3.2441	4.1243	0.0001
NW	SW	5.6625	6.5446	7.4267	0.0002
NW	SE	6.1906	7.0728	9.9549	0.001
NE	SW	2.4203	3.3025	4.1847	0.0004
NE	SE	2.9485	3.8307	4.7129	0.001
SW	SE	-0.3539	0.5282	1.4103	0.4145

In Table (7) the lower p-values ($p < 0.05$) indicate that the mean TCO distributions over different sub-regions have a significant difference. However, the p-value in the last column ($P > 0.05$) demonstrates that there is no significant difference between the mean of South-Western and South-Eastern clusters. This means that we found that there is only three clusters of the mean TCO distributions over Ethiopia. These are North-Western, North-Eastern and Southern clusters as can be seen in Figure (2).

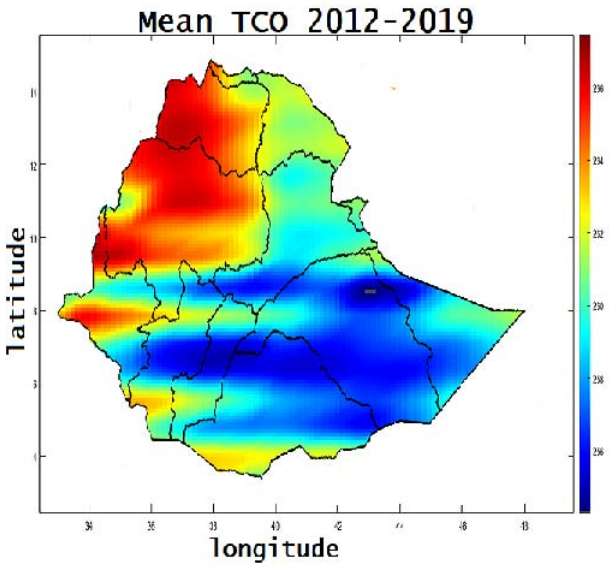

Figure 2 Spatial distribution of Mean TCO.

Figure (2) shows high mean TCO concentration over the Northern part of Ethiopia and low concentration over the southern part of Ethiopia. This overall local increasing TCO variation result along latitude is inline with the global spatial TCO variation study (Stein, 2007). Moreover, we see that the overall three clusters of mean TCO over Ethiopia obtained through the proposed method are similar with the overall mean Rainfall distribution over Ethiopia (Berhanu et al., 2016; Wagesho et al., 2013). From Figure (2), it also seams that the mean TCO distributions looks inversely proportional with the surface temperature distributions over Ethiopia. However, the relation between TCO distributions with meteorological variables over the region might need a thorough investigation with state-of-the-art methods like Graeco-Latin square and we leave this for a subsequent study.

3.3 TCO Concentration over Seasons

We have studied the seasonal TCO concentration over the study area by considering the overall temporal mean of every data point for all the four seasons of Ethiopia including winter, spring, autumn and summer. Fig. 3 shows the temporal distribution of TCO over Ethiopia.

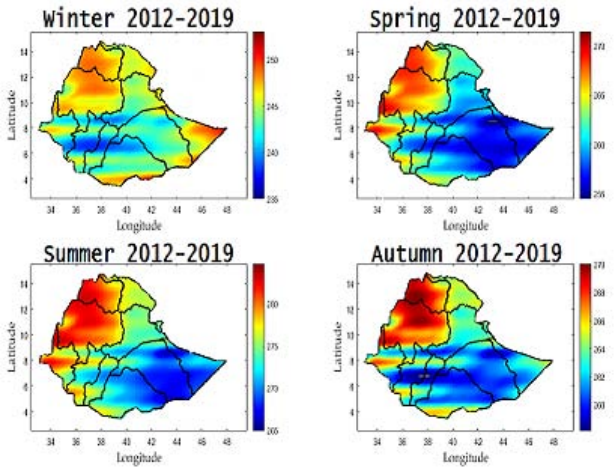

Figure 3 Seasonal distribution of mean TCO over Ethiopia from 2012-2019 , a: Winter(DJF), b: Spring(MAM), c: Summer(JJA), and d= Autumn(SON).

Figure (3) shows the seasonal TCO concentration variations over Ethiopia. We can see that a relative maximum TCO concentration has been observed during the Summer (JJA) and minimum concentration during the Winter (DJF) season. High latitude regions have a relative maximum TCO while low latitude ones experienced minimum values. A relatively minimum values were recorded at higher latitudes & maximum at lower latitudes during Autumn

The variability of TCO concentration over the study area have assessed by calculating the coefficient of variation for each data point as shown in Figure (4) using the overall mean TCO reference value.

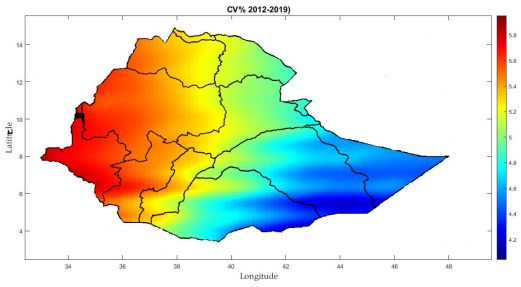

Figure 4 Spatial pattern of coefficient of variation (CV)

Figure 4 shows the variability of TCO concentration during the study period and it is found to be between 4.75% and 5.7%. One can see a relatively lower variations the South-Western part of Ethiopia. The mean TCO concentration in the Northern and Central parts of Ethiopia is relatively higher than the concentration in most of the Southern parts of Ethiopia.

3.4 Minimum TCO Concentration

The global mean ozone concentration is approximately 300 DU (Berbert et al., 1977). We have found that the mean TCO concentration over the study area was

below this global average. In the study period considered, the concentration of TCO was found to be in the range between 216-301 DU, where some are below the threshold concentration 220 DU though the frequency is insignificant. These low TCO values can be a concern and an indication to explore mitigation strategies. Also,it is useful to apply more reliable spatiotemporal analysis technique to investigate TCO concentrations in the region. It is important to notice that a value of 220 DU is considered as the baseline value for an indicator of ozone hole formation (Berbert et al., 1977; Standard, 2019). We have found that some recorded values below this baseline in the study area and need to be considered seriously. Figure (5) depicts the minimum TCO concentration and corresponding date of occurrence.

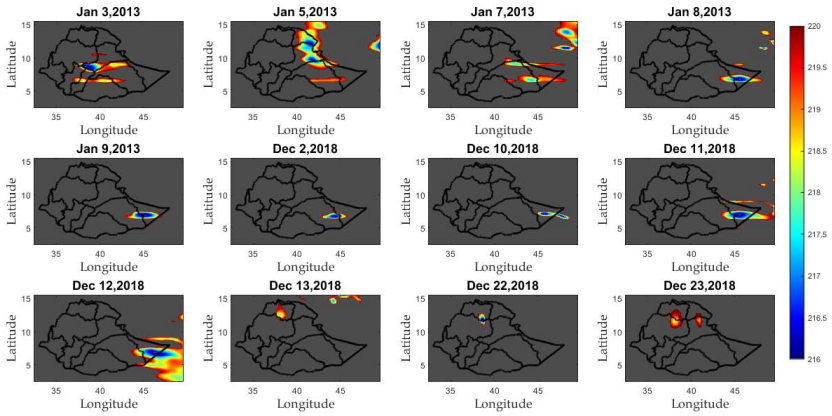

Figure 5 The spatiotemporal distribution of minimum TCO Concentration

Figure 5 shows that TCO concentration is minimum and below the baseline for ozone hole formation in Ethiopia for winter seasons in the study period. Although the frequency is low, we have seen that the recorded values for ozone concentration are significantly lower than those reported in (Berbert et al., 1977).

Based on this study and the results of other researchers over Kenya, West Africa, and Pakistan (Rafiq et al., 2017),(Songa, 2017),(Madhu et al., 2016),(Oluleye and Okogbue, 2013), the source of seasonal variability of ozone distribution over Ethiopia may be mainly due to ozone transport and chemistry. However, in order reach a more strong conclusion, the impact of Quasi Benian Oscillation (QBO) and Solar UV radiation on the variability of ozone over Ethiopia should be studied in detail.

3.5 Temporal TCO Distribution

In order to analyze the temporal characteristics of TCO over the three clusters, we assess the mean, standard deviation, and coefficient of variation and it is given in Table (8).

Table (8) shows that the mean TCO concentration was $264.29DU$, $261.0DU$ and $258.73DU$ over North-Western, North-Eastern, Southern clusters respectively. Moreover, the overall mean TCO of Ethiopia was found to be and $261.35DU$. The concentration of TCO clearly shows an increasing trend with latitudinal changes from South to North which is consistent with the previous studies carried out in other regions (Krueger, 1989; London, 1985; Rafiq et al., 2017).

Table 8 Mean, Coefficient of relative variation and Coefficient of variation over all sub-regions

Region	Mean TCO(DU)	std	CV%
NW	264.29	13.6	5.15
NE	261.0	13.73	5.26
SO	258.73	11.28	4.36
ETH	261.35	12.62	1.07

3.5.1 Timeseries Analysis

We investigated the seasonal nature and trend of ozone distributions through time-series analysis. This is carried out by decomposing the daily timeseries data into trends, seasonal variations, and residual components for each cluster regions independently. The time-series data can be modeled as an additive form due to its similar seasonal effect in each year (Dodge and Commenges, 2006).

In order to assess the long term monotonic trend, first we have defined a 5% threshold with null hypothesis as there is no monotonic trend and we have applied non-parametric Mann-Kendall trend test.

Table 9 Mann-Kendall trend test result over the three clusters

	Clusters NWC	NEC	SOC
N	2890	2890	2890
S-val	-422952	-401190	-230736
Z-stat	-8.1649	-7.7448	-4.4543
P-val	< 0.0001	< 0.0001	< 0.0001

The P-value of < 0.05 in Table (9) indicates the rejection of the null hypothesis H0: and it reveals the existence of monotonic trend over all the three clusters. The long term increasing or decreasing pattern of TCO timeseries have been modeled using linear trend in Africa ((Oluleye and Okogbue, 2013)). In this study as well, we assumed a linear trend defined by equation (10). The average daily TCO data and the corresponding linear fitted line is summarized as follows.

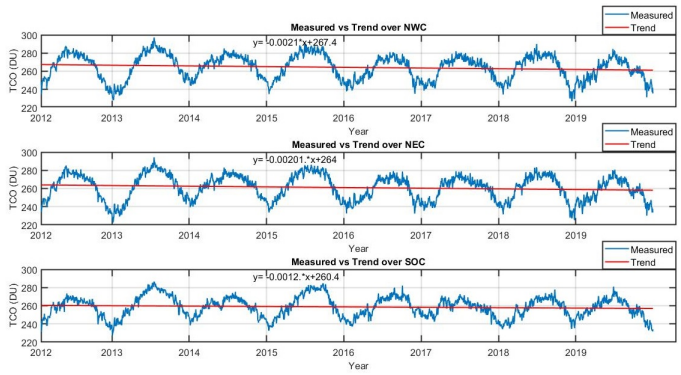

Figure 6 Daily TCO timeseries data with a fitted line over a) North-Western, b) North-Eastern & c) Southern clusters of Ethiopia

We obtained the linear trend equations corresponding to each cluster TCO time-series as $y_{nw} = -0.0021x+267.4$, $y_{ne} = -0.00201x+264$, and $y_s = -0.0012x+260.4$

for monthly ozone concentration over the North-Western, North-Eastern and Southern clusters of Ethiopia, respectively. We have given in Figure (6) TCO timeseries plots together with the fitted trends for each cluster. In all the cases, the results show a decreasing trend with a depletion rate of 0.77 DU/yr, 0.73 DU/yr, and 0.43 DU/yr over North-Western, North-Eastern and Southern parts of Ethiopia respectively. Removing the trend component from the TCO timeseries gives a cyclic component around the time axis as expected. We have given the de-trended data plot in Figure (7) for illustration purpose.

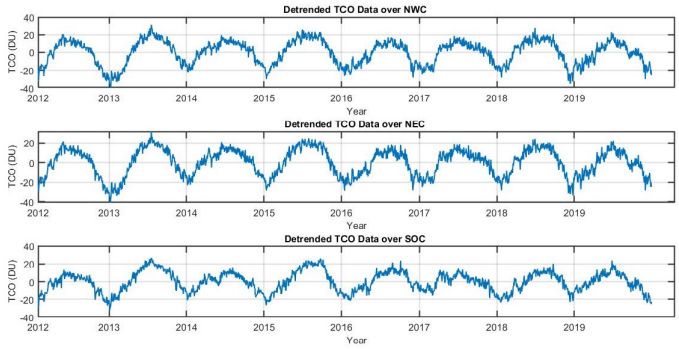

Figure 7 Monthly De-trended Data a) North-Western, b) North-Eastern & c) Southern clusters of Ethiopia

The trend of the TCO variations cannot be identified easily because of the seasonal cyclic variations (Antón et al., 2011). In this study we have detected the period of seasonal pattern by using two different techniques. Visual inspection of timeseries plot as indicated on Figure 8 can be considered as one option.

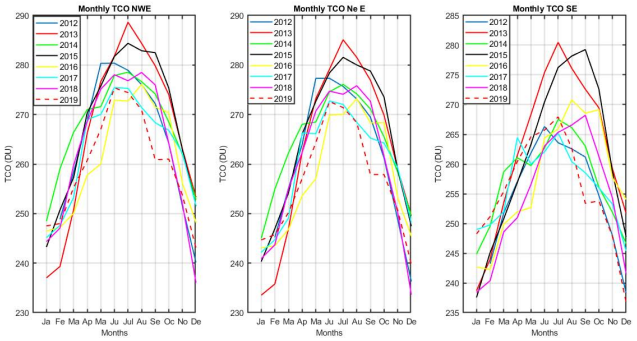

Figure 8 Monthly Mean TCO over clusters

From the sequences of timeseries data plots in Figure 8, the concentration over all of the sub-regions was highest during June, July, and August. It also shows the concentration decreases until December and then rises continuously to July, and hence the annual cyclic behavior is observed. On the other hand, the seasonality of TCO is estimated from the best fit of daily TCO timeseries ((Antón et al., 2011; Fioletov et al., 2008)). We also estimated the cyclic variability of TCO by best fitting

of de-trended data through Fourier series model given by equation 11. In order to identify the dominant frequencies of a timeseries, we used a power spectrum Fast Fourier Transform on our de-trended data which is given in terms of frequency instead of period as indicated in Figure. 9.

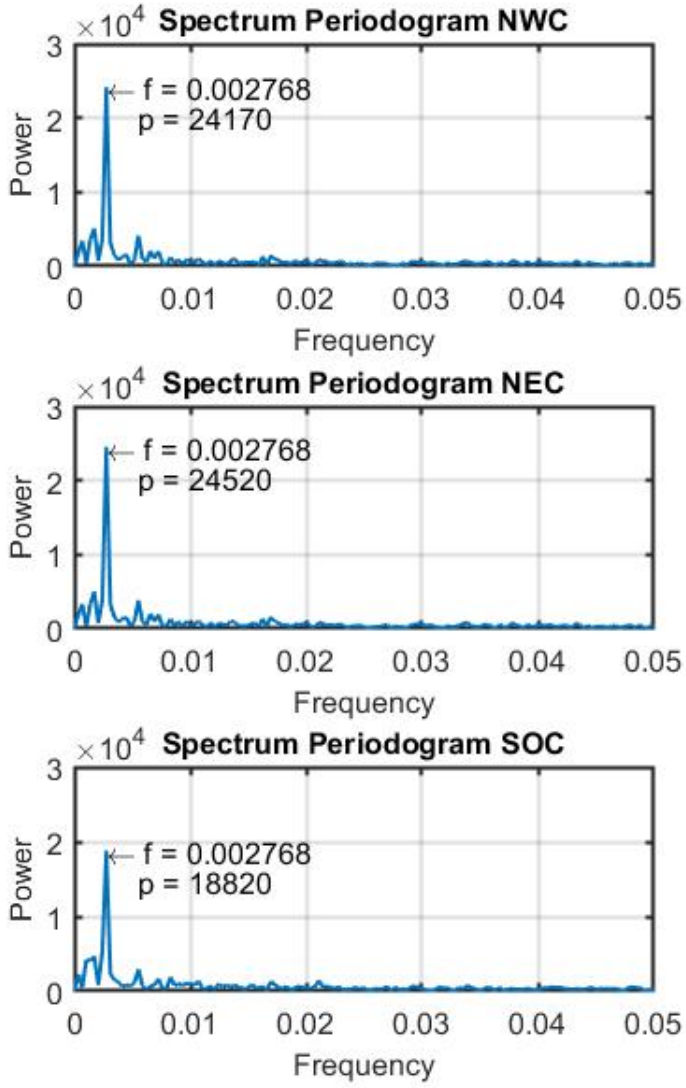

Figure 9 spectral periodogram a)NWC, b) NEC & c) SOC of Ethiopia

The spectral periodogram plot shows that there is a single Fourier power peak with the corresponding frequency $f = 0.002768Hz$ for all clusters. The inverse of this frequency, which is period of the annual cyclic behavior, is 365.25 days. This result is in line with the previous studies by (Antón et al., 2011; Chen et al., 2014;

Fioletov et al., 2008; Vigouroux et al., 2015).

Table 10 Tests of goodness of fit for seasonal components

Cluster		Fourier terms(n) n = 1	n = 2
NW	R^2	0.7865	0.8090
	RMSE	6.2338	5.9002
NE	R^2	0.7959	0.8146
	RMSE	6.1597	5.8741
SO	R^2	0.6835	0.7007
	RMSE	6.3229	6.1536

Table 10 shows that for a Fourier term n = 1: the coefficients of determination (R^2) are 0.7865, 0.7959, and 0.6835 for North-Western, North-Eastern and Southern clusters respectively. In North-Western and North-Eastern clusters the coefficient of determination (R^2) is higher than 0.7 and it is considered as a good seasonal fit (Akoglu, 2018). However, the coefficient of determination (R^2) for Southern cluster was lower than 0.7 and its coefficient of determination (R^2) for n=2 is higher than 0.70. In this case, we used n=1 for North-Western & North-Eastern clusters while n=2 for Southern cluster.

The equations for the seasonality component becomes $S_t = \alpha_1 \cos(\frac{2\pi t}{365.25}) + \beta_1 \sin(\frac{2\pi t}{365.25})$ for North-Western & North-Eastern clusters and

$S_t = \alpha_1 \cos(\frac{2\pi t}{365.25}) + \beta_1 \sin(\frac{2\pi t}{365.25}) + \alpha_2 \cos(\frac{4\pi t}{365.25}) + \beta_2 \sin(\frac{4\pi t}{365.25})$, for Southern cluster. The estimated parameters are presented in Table **??**T12.

Table 11 Parameter Estimation for seasonal components

Cluster	Estimates α_1	β_1	α_2	β_2
NW	-16.85	3.843		
NE	-16.56	3.852		
SO	-13.14	1.616	-1.344	1.512

Table 10 shows that we have a Fourier transform term of n = 1 for North-Western & North-Eastern clusters while n = 2 for Southern cluster. In this case, the fitting functions become

$S_t = -16.85 \cos(\frac{2\pi t}{365.25}) + 3.843 \sin(\frac{2\pi t}{365.25})$,

$S_t = -16.56 \cos(\frac{2\pi t}{365.25}) + 3.852 \sin(\frac{2\pi t}{365.25})$, and

$S_t = -13.14 \cos(\frac{2\pi t}{365.25}) + 1.616 \sin(\frac{2\pi t}{365.25})$

$- 1.344 \cos(\frac{4\pi t}{365.25}) + 1.512 \sin(\frac{4\pi t}{365.25})$ with a coefficient of determination (R^2) of 0.7865, 0.7959, and 0.7007 for North-Western, North-Eastern and Southern clusters respectively.

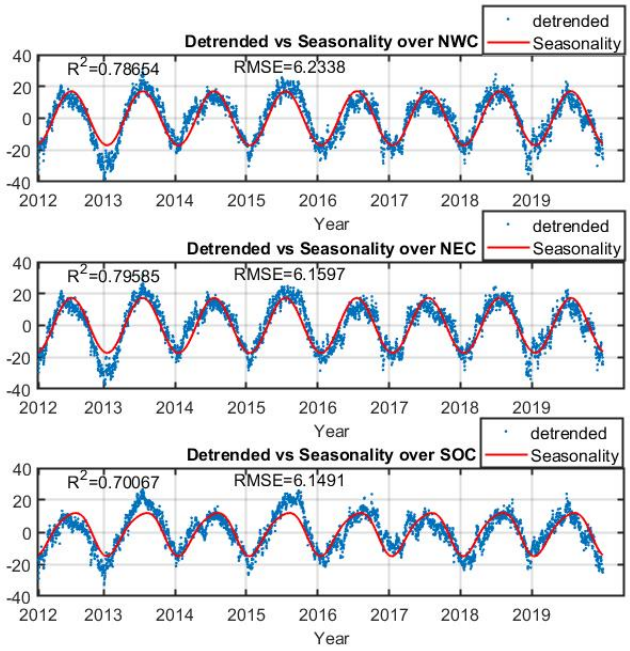

Figure 10 de-trended and seasonal components over a) North-Western, b) North-Eastern & c) Southern clusters of Ethiopia

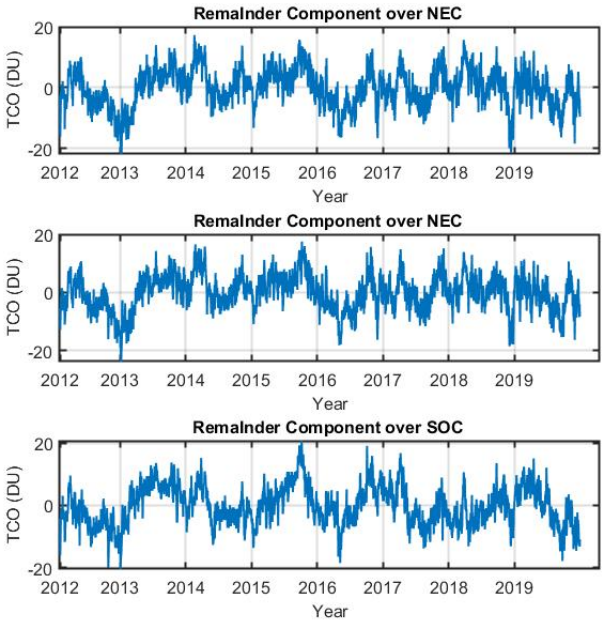

Figure 11 de-trend and seasonally adjusted components a) North-Western, b) North-Eastern & c) Southern clusters of Ethiopia

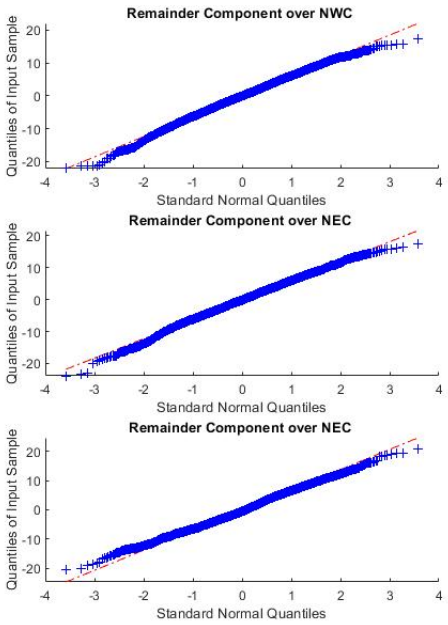

Figure 12 QQ plot for Remaining Components a) Northwestern, b) Northeastern & c) Southern clusters of Ethiopia

The timeseries analysis for this study gives the following model.

$Y_t = \gamma x + \alpha_0 + \alpha_1 \cos(\frac{2\pi t}{365.25}) + \beta_1 \sin \frac{2\pi t}{365.25} + \varepsilon(t)$ for North-Western & North-Eastern clusters, while $Y_t = \gamma x + \alpha_0 + \alpha_1 \cos(\frac{2\pi t}{365.25}) + \beta_1 \sin \frac{2\pi t}{365.25} + \alpha_2 \cos(\frac{4\pi t}{365.25}) + \beta_2 \sin \frac{4\pi t}{365.25} + \varepsilon(t)$ for Southern cluster, where α_0 is the intercept, γ is the annual trend and $\alpha_1, \alpha_2, \beta_1 \& \beta_2$ describes the ozone seasonal cycle.

In order to evaluate the reliability of these models in describing the data, we investigate the residuals of the models if they resemble white noise. The normal probability quantile-quantile plot of the standardized residual given in Figure (12) shows that the residuals can be regarded as Gaussian without any signs of large outliers.

4 Conclusion

We have studied the spatiotemporal distribution of total column ozone concentration over Ethiopia using OMPS satellite data from 108 data points over Ethiopia for the period of 2012-2019. The study has shown that the maximum total column ozone concentration occurred during summer seasons, while the minimum measurements were recorded during the winter seasons on the North-Western and Central Ethiopia. The annual mean total column ozone concentration during the study period is found to be (261.28 ± 4.2)DU. The maximum total column ozone of 301 DU was observed on 18 August 2013 while the minimum of 216 DU was measured on on January 03, 2013.

We have also showed through spatial data clustering study that that the spatial distribution of the total column ozone concentration over Ethiopia can be classified into three major representative clusters: Southern Cluster ($3.5^\circ N$ to $8.5^\circ N$ & $32.5^\circ E - 47.5^\circ E$), North-Eastern Cluster ($9.5^\circ N$ to $14.5^\circ N$ & $41.5^\circ E$ to $47.5^\circ E$) and North-Western Cluster ($9.5^\circ N$ to $14.5^\circ N$ & $32.5^\circ E$ to $40.5^\circ E$). Our TCO time-series analysis has shown a decreasing linear trend in TCO with a depletion rate of 0.77 DU/yr, 0.73 DU/yr, and 0.43 DU/yr over North-Western,North-Eastern & Southern clusters of Ethiopia respectively. We also found a single power peak with the frequency of $f = 0.002768Hz$ with annual cyclic behavior of $\frac{1}{f} \approx 365.25$ days from spectral periodogram for the three clusters.

Declarations

Abbreviations

TCO: total column ozone; OMPS: Ozone Mapper and Profiling Suite Satellite; DU: Dobson Unit; NW:North-Western; NE:North-Eastern; So:Southern

Availability of data and material

The data used in this study can be found freely online from NASA Goddard Space Flight Center Website https://www.esrl.noaa.gov/gmd/grad/neubrew/SatO3DataTimeSeries.jsp

Competing interests

The authors declare that they have no competing interest.

Funding

Not applicable

Authors' contributions

ABA and AMS designed the presented idea, took the lead in writing the manuscript and conducted overall analysis,, with support from all the authors. BDY and UJPR contributed to expanding the main conceptual idea and interpreting the results. In addition to this, all authors have discussed the results and reviewed the manuscript. They have also approved the final manuscript.

Acknowledgements

We gratefully acknowledge the National Aeronautics and Space Administration (NASA) Goddard Space Flight Center for the free use of TCO data.

Author details

[1]Bahir Dar University, Collage of Science, Department of Physics, Ethiopia. [2]Bahir Dar University,College Science,Department of Mathematics, Bahir Dar, Ethiopia,. [3]Ethiopian Institute of Textile and Fashion Technology, Bahir Dar University, Bahir Dar, Ethiopia, , , .

References

Akoglu, H. (2018). User's guide to correlation coefficients. *Turkish Journal of Emergency Medicine*, 18(3):91–93.

Antón, M., Bortoli, D., Costa, M. J., Kulkarni, P. S., Domingues, A. F., Barriopedro, D., Serrano, A., and Silva, A. M. (2011). Remote Sensing of Environment Temporal and spatial variabilities of total ozone column over Portugal. *Remote Sensing of Environment*, 115(3):855–863.

Anwar, F., Chaudhry, F. N., Nazeer, S., Zaman, N., and Azam, S. (2016). Causes of Ozone Layer Depletion and Its Effects on Human: Review. *Atmospheric and Climate Sciences*, 06(01):129–134.

Aucamp, P. J., Björn, L. O., and Lucas, R. (2011). Questions and answers about the environmental effects of ozone depletion and its interactions with climate change: 2010 assessment. *Photochemical & Photobiological Sciences*, 10(2):301–316.

Bais, A., Lubin, D., Arola, A., Bernhard, G., Blumthaler, M., Chubarova, N., Erlick, C., Gies, H., Krotkov, N., Lantz, K., et al. (2006). Surface ultraviolet radiation: past, present, and future. *Scientific assessment of ozone depletion*, 7(21):2007.

Berbert, J., Brownd, J., Felsentreger, T., Harris, D., Johnson, T., Khan, M., Lerch, F., Marsh, J., Murphy, J., Putney, B., et al. (1977). National aeronautics and space administration/goddard space flight center. *NASA Special Publication*, 365:293.

Berhanu, B., Seleshi, Y., Demisse, S. S., and Melesse, A. M. (2016). Bias correction and characterization of climate forecast system re-analysis daily precipitation in ethiopia using fuzzy overlay. *Meteorological Applications*, 23(2):230–243.

Boulis, C. and Ostendorf, M. (2004). Combining multiple clustering systems. In *European Conference on Principles of Data Mining and Knowledge Discovery*, pages 63–74. Springer.

Chen, L., Yu, B., Chen, Z., Li, B., and Wu, J. (2014). Investigating the temporal and spatial variability of total ozone column in the yangtze river delta using satellite data: 1978–2013. *Remote Sensing*, 6(12):12527–12543.

Chipperfield, M. (2003). A three-dimensional model study of long-term mid-high latitude lower stratosphere ozone changes. *Atmospheric Chemistry and Physics*, 3(4):1253–1265.

Dittman, M. G., Ramberg, E., Chrisp, M., Rodriguez, J. V., Sparks, A. L., Zaun, N. H., Hendershot, P., Dixon, T., Philbrick, R. H., and Wasinger, D. (2002). Nadir ultraviolet imaging spectrometer for the npoess ozone mapping and profiler suite (omps). In *Earth Observing Systems VII*, volume 4814, pages 111–119. International Society for Optics and Photonics.

Dodge, Y. and Commenges, D. (2006). *The Oxford dictionary of statistical terms*. Oxford University Press on Demand.

Fioletov, V., Labow, G., Evans, R., Hare, E., Köhler, U., McElroy, C., Miyagawa, K., Redondas, A., Savastiouk, V., Shalamyansky, A., et al. (2008). Performance of the ground-based total ozone network assessed using satellite data. *Journal of Geophysical Research: Atmospheres*, 113(D14).

Hamada, M. and Wu, J. (2000). *Experiments: planning, analysis, and parameter design optimization*. Wiley New York.

Kambezidis, H., Katevatis, E., Petrakis, M., Lykoudis, S., and Asimakopoulos, D. (1998). Estimation of the linke and unsworth–monteith turbidity factors in the visible spectrum: application for athens, greece. *Solar Energy*, 62(1):39–50.

Krueger, A. J. (1989). The global distribution of total ozone: Toms satellite measurements. *Planetary and Space Science*, 37(12):1555–1565.

Kutner, M. H., Nachtsheim, C. J., Neter, J., Li, W., et al. (2005). *Applied linear statistical models*, volume 5. McGraw-Hill Irwin New York.

Libiseller, C., Grimvall, A., Waldén, J., and Saari, H. (2005). Meteorological normalisation and non-parametric smoothing for quality assessment and trend analysis of tropospheric ozone data. *Environmental monitoring and assessment*, 100(1-3):33–52.

Liu, X., Bhartia, P., Chance, K., Spurr, R., and Kurosu, T. (2010). Ozone profile retrievals from the ozone monitoring instrument. *Atmospheric Chemistry and Physics*, 10(5):2521–2537.

LoConte, N. K., Brewster, A. M., Kaur, J. S., Merrill, J. K., and Alberg, A. J. (2018). Alcohol and cancer: a statement of the american society of clinical oncology. *J Clin Oncol*, 36(1):83–93.

London, J. (1985). The observed distribution of atmospheric ozone and its variations. *IN: Ozone in the free atmosphere. New York, Van Nostrand Reinhold Co., 1985, p. 11-80.*, pages 11–80.

Madhu, V. et al. (2016). Madden julian oscillations in total column ozone, air temperature and surface pressure measured over cochin during summer monsoon 2015. *Open Journal of Marine Science*, 6(02):270.

Ogunniyi, J. and Sivakumar, V. (2018). Ozone climatology and its variability from ground based and satellite observations over irene, south africa (25.5 º s; 28.1 º e)-part 2: Total column ozone variations. *Atmósfera*, 31(1):11–24.

Oluleye, A. and Okogbue, E. C. (2013). Analysis of temporal and spatial variability of total column ozone over west africa using daily toms measurements. *Atmospheric Pollution Research*, 4:387–397.

Rafiq, L., Tajbar, S., and Manzoor, S. (2017). Long term temporal trends and spatial distribution of total ozone over pakistan. *The Egyptian Journal of Remote Sensing and Space Science*, 20(2):295–301.

Rex, M., Salawitch, R., von der Gathen, P., Harris, N., Chipperfield, M., and Naujokat, B. (2004). Arctic ozone loss and climate change. *Geophysical Research Letters*, 31(4).

Schmalwieser, A. W., Schauberger, G., and Janouch, M. (2003). Temporal and spatial variability of total ozone content over central europe: analysis in respect to the biological effect on plants. *Agricultural and forest meteorology*, 120(1-4):9–26.

Sivasakthivel, T. and Reddy, K. (2011). Ozone layer depletion and its effects: a review. *International Journal of Environmental Science and Development*, 2(1):30–37.

Songa, C. M. M. (2017). *Modeling the Solar Forcing of the Total Column Ozone Variation in Selected Cities in Kenya*. PhD thesis, COPAS, JKUAT.

Staehelin, J., Harris, N., Appenzeller, C., and Eberhard, J. (2001). Ozone trends: A review. *Reviews of Geophysics*, 39(2):231–290.

Standard, J. M. (2019). Physical chemistry project 3: Chlorine oxides and ozone depletion. *Physical Chemistry*.

Stein, M. L. (2007). Spatial variation of total column ozone on a global scale. *The Annals of Applied Statistics*, 1(1):191–210.

Takele Kenea, S., Mengistu Tsidu, G., Blumenstock, T., Hase, F., Von Clarmann, T., and Stiller, G. (2013). Retrieval and satellite intercomparison of o 3 measurements from ground-based ftir spectrometer at equatorial station: Addis ababa, ethiopia. *Atmospheric Measurement Techniques*, 6(2).

Veefkind, J. P., de Haan, J. F., Brinksma, E. J., Kroon, M., and Levelt, P. F. (2006). Total ozone from the ozone monitoring instrument (omi) using the doas technique. *IEEE transactions on geoscience and remote sensing*, 44(5):1239–1244.

Vigouroux, C., Blumenstock, T., Coffey, M., Errera, Q., García, O., Jones, N. B., Hannigan, J. W., Hase, F., Liley, B., Mahieu, E., Mellqvist, J., Notholt, J., Palm, M., Persson, G., Schneider, M., Servais, C., Smale, D., Thölix, L., and De Mazière, M. (2015). Trends of ozone total columns and vertical distribution from ftir observations at eight ndacc stations around the globe. *Atmospheric Chemistry and Physics*, 15(6):2915–2933.

Wagesho, N., Goel, N. K., and Jain, M. K. (2013). Temporal and spatial variability of annual and seasonal rainfall over ethiopia. *Hydrological Sciences Journal*, 58(2):354–373.

Supplementary Files

This is a list of supplementary files associated with this preprint. Click to download.

- GraphicalAbstract.pdf